arXiv:1008.1801v3 [astro-ph.HE] 9 Feb 2011

DESY 10-131

Inverse Compton gamma-rays from Galactic dark matter annihilation: Anisotropy signatures

Le Zhang[1], **Francesco Miniati**[2] **and Günter Sigl**[1]

[1] II. Institut für theoretische Physik, Universität Hamburg, Luruper Chaussee 149, D-22761 Hamburg, Germany

[2] Physics Department, Wolfgang-Pauli-Strasse 27, ETH Zürich, CH-8093 Zürich, Switzerland

Abstract. High energy electrons and positrons from annihilating dark matter can imprint unique angular anisotropies on the diffuse gamma-ray flux by inverse Compton scattering off the interstellar radiation field. We develop a numerical tool to compute gamma-ray emission from such electrons and positrons produced in the smooth host halo and in substructure halos with masses down to $10^{-6}M_{\odot}$. We show that the angular power spectrum from inverse Compton scattering is exponentially suppressed below an angular scale determined by the diffusion length of electrons and positrons. We also find that the total flux and the shape of the angular power spectrum depends sensitively on the spatial distribution of subhalos in the Milky Way. Finally, the contribution from the smooth host halo component to the gamma-ray mean intensity is negligibly small compared to subhalos.

1. Introduction

The existence of nonbaryonic dark matter in modern cosmology is strongly supported by several independent signatures [1], including the cosmic microwave background (CMB), gravitational lensing and large scale structure surveys. However, the nature of dark matter remains a mystery. To reproduce the correct relic density, it is naturally assumed that dark matter is composed of weakly interacting massive particles (WIMPs) such as the supersymmetric neutralino which is one of the most popular candidates [2, 3]. Since the self-annihilation rate is proportional to the dark matter number density squared, potential signals from dark matter annihilation are most likely to be detected in highly dense regions such as the centers of galaxies. It is also expected that the energy released in dark matter annihilation in the early Universe can influence CMB anisotropies. With the high precision CMB data from the WMAP satellite [4], strong constraints on the properties of dark matter can be obtained [5, 6, 7]. A multi-wavelength analysis of dark matter annihilations has been proposed recently in Ref. [8, 9].

Recently, several cosmic ray and gamma-ray experiments provided new windows to detect the signatures of dark matter. In particular, the PAMELA satellite [10] reported an "excess" of the positron fraction above 10 GeV. Also the $e^- + e^+$ spectra above a few hundred GeV from the Fermi-LAT [11] and HESS measurements [12] are significantly harder than expected [13, 14]. These striking observations were often interpreted in terms of dark matter annihilation or decay which can contribute to the flux of high energy electrons and positrons [15, 16, 17, 18, 19, 20]. However, standard astrophysical sources, such as pulsars [21, 22] and supernova remnants [23, 24, 25] also provide a possible explanation for these excesses.

The high energy electrons and positrons induced by WIMP annihilation produce gamma-rays through inverse Compton scattering (ICS) off the low energy background photons in the interstellar radiation field (ISRF) and through bremsstrahlung emissions due to the interaction with the ionized interstellar medium. These components add to the prompt gamma-ray radiation accompanying pairs emitted in the annihilation event [26]. Gamma-ray dark matter signatures could be identified by the Fermi Large Area Telescope [27], due to its unprecedented angular and energy resolution, despite the fact that the gamma-ray spectrum is dominated by conventional astrophysical sources, such as pulsars, supernovas, blazars [28, 29] and perhaps structure formation shocks [30]. Many efforts [31, 32, 33, 34, 35, 36, 37] have been devoted to extract indirect dark matter signatures or to set limits on a large class of WIMP models by investigating the Fermi-LAT diffuse gamma-ray measurements. Especially, a universal model-independent method can be used to place constraints on any dark matter model [38, 39] through convolving *response functions* of signal-to-background with a specific injection energy spectrum of electrons and positrons.

In the WIMP cold dark matter scenario, the dark halos can form at very high redshift, $z \approx 60$, with a minimum mass of $\sim 10^{-6} M_\odot$ [40, 41, 42, 43] determined by the free-streaming limit and collisional damping leading to a cutoff of the primordial power

spectrum. This suggests that if they can survive until the present day, an enormous number of dark matter clumps (subhalos) are expected to be embedded in our Galaxy. Recent numerical simulations [44, 45, 46] confirm this prediction, although the role of the tidal effects from the baryonic component has yet to be quantified and there is no direct test by observations. Nevertheless, several references have discussed the resulting signals pointing out that subhalos can boost annihilation rates and produce a distinct radial distribution of emissions [33, 47, 48, 49, 50].

Alternatively, a statistical analysis of the full-sky emission map can be used to identify dark matter signatures, which can be promising if, e.g., one can identify features in the anisotropy power spectrum that characterize uniquely the dark matter spatial distribution with respect to other astrophysical sources. In this respect, one is interested in quantifying the anisotropy signatures from annihilating dark matter which can be different from those of astrophysical origin particularly at small scales.

The first calculations of this kind were performed analytically for gamma-ray background anisotropies induced by both annihilating extragalactic dark matter halos [51, 52] as well as Galactic subhalos [53]. Analytic calculations were also performed for the anisotropic radio signatures from decaying dark matter [54] and compared with the mean intensity and angular power spectrum of the astrophysical and cosmological radio background.

More recently anisotropies of the diffuse gamma-ray background from annihilating dark matter in galactic subhalos have been computed using a numerical approach in Ref. [55]. According to their results, Fermi-LAT should be sensitive enough to constrain the amount of dark matter substructure through the anisotropy signal discussed above. The same numerical approach as in [55] can be extended to the anisotropies from both the galactic and extragalactic dark matter contributions [56, 57, 58, 59, 60]. In general, however, both the mean flux and anisotropy signal are contaminated by ordinary astrophysical sources including galactic and extragalactic resolved point sources, structure formation shocks [61, 62], and normal galaxies [63, 64]. Removal of such contributions [65], can greatly improve the detectability for searches of dark matter.

All of the above analyses were based on the gamma-rays from direct annihilation into photons. However, the ICS radiation from energetic electron and positron pairs produced by annihilation of dark matter also generates unique gamma-ray signatures, in an energy range that depends on the dark matter model. Thus in the present paper we study the gamma-ray anisotropies produced by this "secondary" emission, which can be regarded as a new target for indirect searches of signatures induced by Galactic substructure halos. The important point is that the properties of the angular anisotropies for emission from secondary electrons and positrons will be different in general than for prompt emission, because the former will be affected by propagation effects in the Galaxy. In fact, by adopting a spatial diffusion model typical for high energy electrons and positrons in the Galaxy, we show that the angular power spectrum is suppressed at small angular scales corresponding to the distance diffusively traveled by the charged particles during their energy loss time. As a result, for a typical dark

matter model with mass of 1 TeV and a canonical thermal freeze-out cross section $3 \times 10^{-26}\mathrm{cm}^3/\mathrm{s}$, the angular power spectrum from inverse Compton scattering peaks at large angular scales.

The remainder of this paper is organized as follows. In Sect. 2, we set up the formalism used in this paper for calculating the mean intensity and angular power spectrum of gamma-rays induced by dark matter annihilation and develop a robust numerical scheme to simulate the small subhalos with masses down to $\sim 10^{-6} M_\odot$. We present the results of our calculations in Sect. 3. Finally, we summary our paper in Sect. 4. We will use natural units in which $c = 1$ throughout.

2. Formalism

2.1. Diffusion models

The propagation of high energy electrons and positrons in the turbulent Galactic magnetic field can be described as a diffusion-energy loss equation [66] for the electron-positron number density n_e, neglecting the convection and re-acceleration terms which are only relevant for electrons and positrons below 10 GeV [67]:

$$\frac{\partial n_e}{\partial t} = \boldsymbol{\nabla} \cdot (D(E, \mathbf{r})\, \boldsymbol{\nabla} n_e) + \frac{\partial}{\partial E} \left(b(E, \mathbf{r})\, n_e \right) + Q(E, \mathbf{r})\,. \tag{1}$$

Here, the spatial diffusion coefficient is taken as $D(E, \mathbf{r}) = D_0 (E/\mathrm{GeV})^\delta$; $b(E, \mathbf{r})$ is the energy loss term and $Q(E, \mathbf{r})$ the source term, both of which are described in more details below. In the following we will often use the term electron as a short hand for both electrons and positrons. With the assumption that spatial diffusion and energy loss coefficients are spatially independent, for a given source distribution and boundary conditions, the propagation equation can be solved analytically. We assume the diffusion zone to be a cylinder with half-height L of a few kpc and radius $R \gtrsim 20\,\mathrm{kpc}$. In this paper, we adopt the widely used MED model which, compared to other models, i.e. the MIN and MAX models, predicts intermediate values for the antiproton flux when fitted to reproduce the B/C ratio [68] with $D_0 = 1.28 \times 10^{27}\mathrm{cm}^2/\mathrm{s}$, $\delta = 0.7$, and the half-height of the diffusion zone $L = 4\,\mathrm{kpc}$. The MIN and MAX propagation models would decrease and increase the predicted gamma-ray fluxes roughly by a factor of three and two, respectively. However, we verified that the shape of the angular power spectrum predicted by these three propagation models is basically the same. Since in the present paper we mainly focus on a new "suppression" feature in angular power spectrum of the gamma-ray component from ICS, we will use the MED model in the following calculations.

In this study, we investigate only the case in which electrons and positrons can escape freely at the boundaries of the diffusion zone. If the diffusion coefficient increases exponentially instead of the free-escape boundary condition, we expect that the angular power spectrum would be modified only at multipoles $l \ll 10$ since the diffusion of electrons and positrons would flatten their distribution at length scales even larger than

the whole diffusion zone. This implies that the angular power spectrum produced in the region of extremely large diffusion coefficient can not significantly influence the signature in the full-sky angular power spectrum we found at $l \sim 10$. In other words, the anisotropies weakly depend on different boundary conditions.

2.1.1. Energy losses At energies above 10 GeV, the dominant energy losses are synchrotron radiation and inverse Compton scattering (ICS) on the interstellar radiation field. Therefore, in the Thomson limit we write $b(E, \mathbf{r}) = b_0\, E^2$ [for a more complicated treatment of energy loss see Ref.[69]], where $b_0 = 3 \times 10^{-16}$GeV/s for starlight (SL) , infrared (IR), CMB photons and a magnetic field of 3μG. The Inter-Stellar Radiation Field (ISRF) can be approximately characterized as a superposition of three blackbody-like spectra with different temperatures and normalization factors relative to a true black-body emitter: one for the CMB with $T_{CMB} = 2.73$K, for the IR with $T_{IR} = 40.61$K and for the SL with $T_{SL} = 3800$K [32]. The typical normalization of the SL and IR fields of radiation depends on the position in the Galaxy. The averaged normalizations of ISRF photon densities per energy used in this paper are $8.9 \times 10^{-13}, 1.3 \times 10^{-5}$ and 1 for SL, IR and CMB, respectively [32]. Although these normalizations are valid only in the region with latitude $20^\circ > |b| > 10^\circ$, we have checked that changing the normalization of the ISRF affects the gamma-ray emissions only weakly because an increased emission is partly compensated by a decrease of the density of electrons and positrons as energy losses increase. We also verified that the deviation from the detailed numerical simulation with Galprop [70] is less than a factor of two for a realistic spatial distribution of the ISRF [71].

2.1.2. Dark matter model In the annihilating dark matter scenario, the source term can be written as

$$Q(\mathbf{r}, E) = \frac{1}{2} \langle \sigma v \rangle \left(\frac{\rho(\mathbf{r})}{m_\chi} \right)^2 f_e(E), \tag{2}$$

where $f_e(E)$ is the annihilation spectrum into electrons and positrons at energy E. For simplicity, we assume mono-energetic injection of the positron and electron in case of CP conservation, namely $f_e = 2\delta(E - m_\chi)$. We choose $m_\chi = 1$TeV, which can well fit the PAMELA excess [15] while not in conflict with gamma-ray observations by Fermi-LAT [32]. Finally, we use $\langle \sigma v \rangle = 3 \times 10^{-26}\mathrm{cm}^3/\mathrm{s}$ to reproduce the correct relic density for thermal freeze-out. By convolving our results for the gamma-ray spectra with the pair energy, our computational approach can be easily adapted to pair spectra different from mono-energetic injection, such as from dark matter annihilating into $\mu^\pm, \tau^\pm$, and $W^\pm$.

2.2. Green's function

As most of the electrons escape towards the $z-$direction, we impose the Dirichlet boundary condition $n(x, y, z = |L|) = 0$, at which the particles can freely escape. We

thus model the diffusion zone as an infinite slab of half thickness L, and we take $L = 4$kpc for the MED diffusion model. The free-space Green's function [33] for Eq. (1) is

$$G_{\rm free}[\mathbf{r}, \mathbf{r}', \lambda_D(E, E')] = \frac{1}{b(E)} \frac{1}{(\pi\lambda_D^2)^{3/2}} {\rm e}^{-(\mathbf{r}-\mathbf{r}')^2/\lambda_D^2} \,, \tag{3}$$

where we have defined the diffusion length as

$$\lambda_D^2(E, E') \equiv 4 \int_E^{E'} \frac{D(E)}{b(E)} dE = 4D_0 \frac{\rm GeV}{b_0} \left(\frac{(E/{\rm GeV})^{\delta-1} - (E'/{\rm GeV})^{\delta-1}}{1-\delta} \right) , \tag{4}$$

which is the average distance e^+e^- diffuse through during their energy loss time. Then, the Green's function satisfying appropriate boundary conditions can be obtained by considering a series of image charges at positions $x_i = x, y_i = y, z_i = (-1)^i z + 2i \cdot L$. One can verify that

$$G_{2L}(\mathbf{r}, \mathbf{r}', \lambda) = \sum_{i=-\infty}^{\infty} (-1)^i G_{\rm free}(\mathbf{r}, \mathbf{r}'_i, \lambda) \tag{5}$$

fulfills the Dirichlet boundary condition. Thus, the general solution to Eq. (1), in the limit of time-independent sources and electron/positron number densities which already reached equilibrium, is given by

$$n_e(\mathbf{r}, E) = \frac{1}{b(E)} \int d^3\mathbf{r}' \int_E^{\infty} dE' G_{2L}(\mathbf{r} - \mathbf{r}', \lambda_D(E, E')) Q(\mathbf{r}', E') \,. \tag{6}$$

For the diffuse gamma-ray emission we are more interested in the column density of electrons,

$$\sigma_e(l, b, E) = \int_0^{l_{max}} d\ell \; n(\mathbf{r}, E) \,, \tag{7}$$

than in the local space density of electrons. The observer is located at the solar system. In galactic coordinates, a point in cartesian coordinates (x, y, z) at a distance ℓ from the observer is given by

$$x = \ell \, \cos b \, \cos l, \tag{8}$$

$$y = \ell \, \cos b \, \sin l, \tag{9}$$

$$z = \ell \, \sin b \,, \tag{10}$$

where l and b are the galactic longitude and latitude, respectively. We truncate the integral in Eq. (7) at the edge of the diffusion zone, beyond which particles are not confined, $z_{max} = L$ or $\ell_{max} = L/|\sin b|$. The line-of-sight integral can directly act on the free Green's function [33],

$$\begin{aligned} G^{\sigma}_{\rm free}(l, b, \mathbf{r}', \lambda_D) &= \int_0^{\ell_{\rm max}} d\ell \, G_{\rm free}(\ell\mathbf{n}, \mathbf{r}', \lambda_D) = \\ &= \frac{e^{[(\mathbf{n}\cdot\mathbf{r}')^2 - (\mathbf{r}')^2]/\lambda_D}}{2\pi\lambda_D^2 b(E)} \left[{\rm erf}\left(\frac{\ell_{\rm max} - \mathbf{n}\cdot\mathbf{r}'}{\lambda_D} \right) - {\rm erf}\left(\frac{-\mathbf{n}\cdot\mathbf{r}'}{\lambda_D} \right) \right] , \end{aligned} \tag{11}$$

where we have defined the unit-vector $\mathbf{n} \equiv \mathbf{r}/\ell$. The Green's function satisfying the boundary condition is thus

$$G^{\sigma}_{2L}(l, b, \mathbf{r}', \lambda) = \sum_{i=-\infty}^{\infty} (-1)^i G^{\sigma}_{\rm free}(l, b, \mathbf{r}'_i, \lambda) \,. \tag{12}$$

The column density of electrons therefore reads

$$\sigma_e(l,b,E) = \frac{1}{b(E)} \int d^3\mathbf{r}' \int_E^\infty dE'\ G_{2L}^\sigma\left[l,b,\mathbf{r}',\lambda_D(E,E')\right] Q(\mathbf{r}',E')\,. \tag{13}$$

In the limit of $\lambda_D \gg r_s$, where r_s is the scale radius of the subhalo profile, the subhalo can be regarded as a point-like source. Eq.(13) can then be simplified to

$$\sigma_e(l,b,E) = \sum_k \frac{1}{b(E)} \int_E^\infty dE'\ G_{2L}^\sigma\left[l,b,\mathbf{r}_k,\lambda(E,E')\right] j_k(\mathbf{r}_k), \tag{14}$$

where $j_k(E) = \int d^3\mathbf{r}\ Q_k(\mathbf{r},E)$ for a given subhalo source Q_k located at $\mathbf{r}_k$. For the largest subhalos with masses larger than $\simeq 10^9 M_\odot$, their radius r_s can be somewhat larger than the diffusion length λ_D. Nevertheless, their contribution to the total flux is a factor $\sim 10^4$ smaller than the flux from the smaller subhalos. Therefore, neither the mean intensity nor the dimensional angular power spectrum (see Sect. 2.6) relies significantly on the distribution of electrons in the largest subhalos. As a result, for our purposes we can apply Eq. (14) to all subhalos even if $r_s > \lambda_D$.

2.3. Halo function

Alternatively, for primary electrons and positrons from the smooth host dark matter halo, the Bessel-Fourier scheme [72, 73] can require less computational time than the Green's function. The electron and positron number density after propagation can be expressed as

$$n_e(r,z,E) = \frac{1}{b(E)} \int_E^{M_\chi} dE'\ f_e(E')\ I(r,z,E,E'), \tag{15}$$

and $I(r,z,E,E')$ is the halo function defined by

$$I(r,z,E,E') = \sum_i \sum_n J_0\left(\frac{\alpha_i r}{R}\right) \sin\left[\frac{n\pi(z+L)}{2L}\right] e^{-\left[\left(\frac{n\pi}{2L}\right)^2 + \frac{\alpha_i^2}{R^2}\right]\frac{\lambda_D^2}{4}} R_{i,n}\,. \tag{16}$$

Here, the α_i are the zeros of the Bessel function J_0 and $R_{i,n}$ are the coefficients of the Bessel-Fourier transform of the source term.

2.4. Diffuse Emission: Inverse Compton spectrum

For relativistic electrons and positrons with energy E up scattering background photons from energy ϵ to E_γ, the emitted inverse Compton power per energy interval is

$$P_{\rm IC}(E_\gamma,E) = E_\gamma \int\ d\epsilon\ n(\epsilon) \frac{d\sigma}{dE_\gamma}(E_\gamma,\epsilon,E)\,, \tag{17}$$

where $n(\epsilon)$ is the differential ISRF photon number density, while the differential cross section $(d\sigma/dE_\gamma)(E_\gamma,\epsilon,E)$ is given by the Klein-Nishina formula [74]. Folding $P_{\rm IC}$ with the spectral distribution of the equilibrium number density of electrons and positrons, we get the emissivity of IC photons of energy E_γ,

$$j_{\rm IC}(E_\gamma) = \int\ dE\ n_e(E)\ P_{\rm IC}(E_\gamma,E), \tag{18}$$

which yields the IC intensity at energy E_γ by the line-of-sight integral

$$I_{\rm IC}(E_\gamma) = \frac{1}{4\pi}\int d\ell\ j_{\rm IC}(E_\gamma, \mathbf{r})\,. \tag{19}$$

According to the Eq. (13), the IC intensity from the electrons and positrons can be simplified to

$$I_{\rm IC}(l, b, E_\gamma) = \frac{1}{4\pi}\int dE\ P_{\rm IC}(E_\gamma, E)\ \sigma_e(l, b, E)\,. \tag{20}$$

There is a well known "delta-function approximation" where an electron with energy E inverse Compton scattering black-body photons with temperature T emits photons with a characteristic energy E_γ in both the Thomson and extreme Klein-Nishina limits [75], *i.e.*, $P_{\rm IC}(E_\gamma, E) = P_{\rm IC}(E)\delta[E_\gamma - E_c(E)]$, where $P_{\rm IC}(E)$ is the total IC energy loss rate of the electron. The numerical calculations show that $E_c(E)$ may be approximated by $E_c(E) \simeq 4k_BT(E/m_e)^2$ and in the Thomson regime one has $P_{\rm IC}(E) = (16e^4\pi/3)u_bE^2/m_e^4$, where e is the electron charge and u_b is the background photon energy density. Eq. (20) can thus be simplified to

$$I_{\rm IC}(l, b, E_\gamma) = \frac{1}{16\pi}\,\sigma_e(l, b, E)\frac{m_eP_{\rm IC}(E)}{\sqrt{E_\gamma k_BT}}\,, \tag{21}$$

where the electron/positron energy E is related to the gamma-ray energy E_γ through the following condition: $E_\gamma = E_c(E)$. This relation reproduces the known slope $I_{\rm IC}(E_\gamma) \propto E_\gamma^{-(s-1)/2}$ for an electron spectrum of $\sigma_e(E) \propto E^{-s}$. In the Thomson limit and for our choice of monoenergetic injection of electron-positron pairs, the index $s \simeq 2$ in the stationary situation if the energy loss term dominates on the right hand side of Eq. (1), as is usually the case for electron energies above 10 GeV. For $E \lesssim$ TeV we are always in the Thomson limit.

2.5. Galactic halo substructure

In the present section we discuss contributions to the source term $Q(\mathbf{r}, E)$ both from the smooth host halo and the individual subhalos. The two most important features of the subhalos are their mass distribution and their spatial distribution. In the following, we briefly summarize the properties of subhalos used in our calculations for which we adopt the same description as in Ref. [55], and references therein.

2.5.1. Subhalo radial distribution There are two widely used scenarios for describing the subhalo radial distribution. One is unbiased relative to the Galactic smooth component (host halo) with the NFW density profile [76] given by

$$\rho_{\rm NFW}(r) = \frac{\rho_s}{x(1+x)^2}\,, \tag{22}$$

with $x \equiv r/r_s$, where r_s is a scale radius and ρ_s is the characteristic density. For the case where the subhalo distribution is anti-biased compared to the smooth component,

we use the fitting formula of the subhalo radial distribution from Gao *et al* [45, 46]. The cumulative fraction of subhalos within a given radius is

$$\frac{N_{anti}(<\zeta)}{N_{tot}} = \frac{(1+a\,c_{200})\,\zeta^{\beta}}{1+a\,c_{200}\,\zeta^{\gamma}}\,, \tag{23}$$

with $\zeta \equiv r/r_{200}$, $a = 0.244$, $\beta = 2.75$, $\gamma = 2$ and $c_{200} \equiv r_{200}/r_s$ is the host halo concentration. Furthermore, N_{tot} is the total number of subhalos within virial radius r_{200} of the host halo. For a host halo with the NFW density profile we adopted $\rho_s = 0.2$ GeV/cm^3, $r_s = 21.7\,$kpc and $c_{200} = 12$ [77].

2.5.2. The subhalo mass function Recent simulations suggest that the cumulative number of subhalos above a given mass M in units of the solar mass can be fitted simply by a power law [78],

$$N(>M) \simeq 64\left(\frac{M}{10^8 M_\odot}\right)^{-\alpha_m}\,. \tag{24}$$

In the present paper, we simulate the subhalos with mass down to around one Earth mass, $M_{\rm min} = 10^{-6}M_\odot$ and choose $\alpha_m = 0.9$, as suggested by simulations. We find that choosing α_m between 0.8 and 1 [55] would change the mean intensity by roughly a factor of 20.

2.5.3. The subhalo density profile More recent simulations suggest that the central structure of dark matter halos deviates from the NFW profile in the innermost regions, which can be well reproduced by an Einasto density profile. Therefore, here we use the Einasto profile with the parameter $\alpha = 0.16$ given by Gao *et al* [45],

$$\rho(r) = \rho_s \exp\left(\frac{2}{\alpha}\right)\exp\left[-\frac{2}{\alpha}\left(\frac{r}{r_s}\right)^{\alpha}\right]\,. \tag{25}$$

The relation of halo concentration and mass is given by

$$c(M) = 398.1\left(\frac{M}{M_\odot}\right)^{-0.138}\,. \tag{26}$$

The slope and normalization are consistent with those found by Bullock *et al* [79].

2.6. The angular power spectrum

The angular power spectrum of the emission maps can be calculated by using the public HEALPix package [80]. We define the dimensionless quantity $\delta I(\psi, E_\gamma) \equiv (I(\psi, E_\gamma) - \langle I\rangle)/\langle I\rangle$ as a function on the sphere, which can be expanded in spherical harmonics Y_{lm} as

$$\delta I = \sum_{l=0}^{l_{max}}\sum_{m=-l}^{l} a_{lm}Y_{lm}(\psi)\,, \tag{27}$$

where I(ψ) describes the gamma-ray intensity in the direction ψ. The *dimensionless* angular power spectrum of δI is given by the coefficients

$$C_l = \frac{1}{2l+1} \sum_{m=-l}^{l} |a_{lm}|^2 \,. \tag{28}$$

Note that the measured dimensional amplitude C_l^I of the total angular power spectrum in units of intensity squared can be obtained by multiplying the dimensionless angular power spectrum of a given component, $C_{l,i}$, with its mean intensity squared, $\langle I_i \rangle^2$ and summing over the components,

$$C_l^I = \sum_i \langle I_i \rangle^2 C_{l,i} \,, \tag{29}$$

where in our case the sum basically runs over the contributions of the smooth host halo, the subhalo distribution and other astrophysical foregrounds and backgrounds. Here we assumed that the different contributions are uncorrelated.

2.7. Numerical scheme

In numerical calculations, taking into account subhalos down to masses $\sim 10^{-6} M_\odot$ in the angular power spectrum would require the generation of $\sim 10^{16}$ subhalos within the diffusion zone in a given Monte Carlo realization. This is not very practical and severely limits the number of realizations one can simulate. Thus, we need to develop a sound scheme to circumvent these computational limits. Here we take advantage of a few simple facts: (i) Two terms contribute to the fluctuation anisotropies in units of average intensity squared; the one-subhalo term (C_{1h}^I) which is Poissonian noise and the two-subhalo term (C_{2h}^I) due to the cross-correlation of substructure arising from their radial distribution within the host halo (see Eqs. (19) and (20) of Ref. [53])). (ii) Qualitatively speaking, the two-subhalo term scales linearly with the square of the average flux whereas the one-subhalo term is proportional to an integral of squared luminosities of subhalos. Since subhalo luminosity L_{sub} is related to its mass M via $L_{sub} \propto \int dV_{sh} \rho_{sh}^2(r, M) \approx Mc(M)^3$, by using Eq. (26), the correlation between gamma-ray luminosity and mass thus is positive, i.e., $L_{sub} \propto M^{0.6}$. One-subhalo term and two-subhalo term per decade of subhalo mass then can be estimated as $C_{1h}^I \propto dN/d\log(M) L_{sub}^2 \approx M^{0.3}$ and $C_{2h}^I \propto (dN/d\log(M) L_{sub})^2 \approx M^{-0.6}$. Therefore, large and relatively rare substructures dominate the one-subhalo term, but negligibly to the two-subhalo term, and the small but numerous substructure halos dominate the two-subhalo term.

There is thus a dividing mass of substructures, M_0, below which their contribution to one-subhalo term are negligible. The numerical value of this mass depends on the assumed radial distribution of the substructure halos (see below). In any case, it turns out that halos with $M < M_0$ have a characteristic radius, r_s, much smaller than the diffusion length of the gamma-ray emitting electrons, i.e. $\lambda_D \gg r_s$. Thus, effectively all halos below M_0 have the same image on the sky in ICS with a characteristic size given by λ_D. This further simplifies our calculations because besides minor poissonian noise, the

angular power spectrum from subhalos with $M < M_0$ is simply obtained by convoluting the subhalo spatial distribution with the mass-independent ICS subhalo image. Thus the contribution from subhalos with $M < M_0$ is taken into account straightforwardly as follows: We generate a distribution of subhalos with mass in the decade $10^{-6} - 10^{-5} M_\odot$ to obtain the full-sky map.

The number of generated subhalos is typically much smaller than the actual value, $N(10^{-6} < M/M_\odot < 10^{-5})$, but is sufficiently large that the two-subhalo term divided by the mean intensity squared has converged. The intensity of the map and the corresponding two-subhalo term thus can be rescaled to the value appropriate for $N(10^{-6} < M/M_\odot < M_0)$ halos. In this way, the simulated two-subhalo term of the angular power spectrum can fairly approach the actual one.

Since the one-subhalo term is not linearly proportional to the square of the average intensity and is contributed mostly by larger subhalos, we thus complete the calculation by adding the contribution of subhalos with mass $M > M_0$, which can now be done with a direct Monte Carlo simulation. Specifically, we find that our calculation of the angular power spectrum reaches convergence when we use at least 10^5 subhalos for each mass decade from $10^{-6} M_\odot$ to M_0 within the diffusion zone, when we use $M_0 = 10^4 M_\odot$ for the unbiased radial distribution and $M_0 = 10^2 M_\odot$ for the anti-biased case.

Note that this method can not be applied to the angular power spectrum of the direct annihilation component since in this case the profile of the emitting region depends on the profile of each subhalo rather than on the identical diffusion length which just depends on the energy of electrons and positrons for all subhalo masses.

3. Results for Galactic Dark Matter

In this section, we make use of the formalism derived in the previous section to compute the gamma-ray mean intensity map and associated anisotropy power spectrum due to both the smooth host halo component and the substructure halos. We also study how the map morphology and anisotropies depend on the radial distribution of subhalos and of the gamma-ray energy.

3.1. Diffuse Gamma-ray Emission

We first consider the gamma-ray emission produced by dark matter annihilating into e^+e^- pairs scattering off the ISRF both in the smooth host halo and the subhalos. Using the formalism developed in Sect. 2, the fluxes from the smooth host halo at 1 GeV, 10 GeV and 100 GeV are shown in Fig. 1. Here we use galactic coordinates, where an observer is located at 8.5 kpc from the Galactic center. We adopt the NFW density profile with the parameters given in Sect. 2.5, and find, as expected, that most of the signal comes from the central Galactic region where the dark matter is highly concentrated. The values of the mean gamma-ray intensity from both the host halo and the substructure are also reported in Tab. 1 for the above three photon

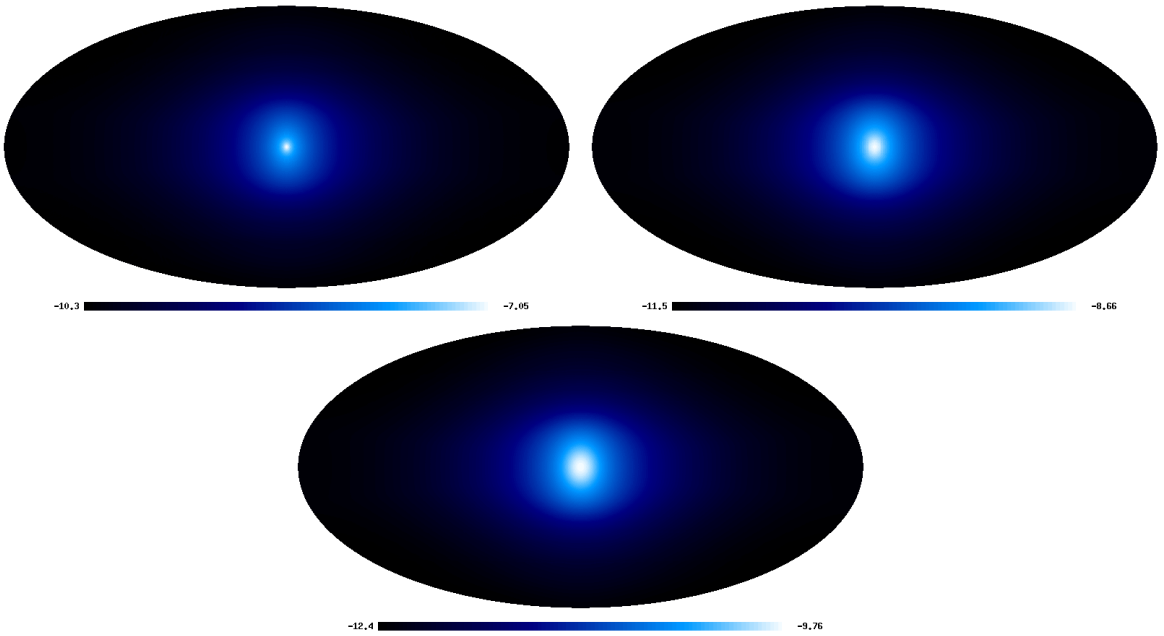

Figure 1. Sky maps of gamma-ray emission in Galactic coordinates at 1 GeV (top-left), 10 GeV (top-right) and 100 GeV (bottom) due to ICS from the host halo. The color scaling is logarithmic, and the unit is $1/\mathrm{s/cm^2/sr}$.

energies. We find that in both cases the mean gamma-ray intensity decreases faster than $\sim E_\gamma^{-1/2}$ in Eq. (21). This is because there will be a high energy cut-off in E_γ once the required energy of the parent pairs $E \simeq m_e[E_\gamma/(4k_BT)]^{1/2}$ scattering off the low energy background photons exceeds the maximum energy M_χ produced by dark matter annihilation. The effect is even stronger when the delta-function approximation for ICS is assumed, as in our case. As a consequence, all background photon energies at CMB energies and above contribute to the 1 GeV ICS photon flux, whereas only the IR and SL contribute to the 10 GeV photon flux and only the SL contributes to the 100 GeV photon flux, as also summarized in Tab. 2. Furthermore, using the relation between E and E_γ and the expression for $P_{\rm IC}(E)$, for an electron spectrum $\sigma_e \propto E^{-s}$ Eq. (21) gives the scaling $I_{\rm IC}(E_\gamma) \propto u_b E_\gamma^{(1-s)/2} T^{(s-3)/2}$. Using the different normalizations for the CMB, IR and SL densities, then would suggest that the gamma-ray intensity originating from e^+e^- pairs scattering off CMB photons is about 5 times larger than the one from scattering off the IR photons and about 10 times lager than the contribution from scattering off SL photons, provided there is no restriction from the kinematics. However, the e^+e^- pairs produced by annihilating dark matter do have an absolute cutoff at the parent particle energy. As a result, the more detailed numerical results show that most of the gamma-ray intensity at 1 GeV is produced by pairs with $E \simeq 526$ GeV scattering off the CMB, whereas pairs with $E \simeq 431$ GeV scattering off IR photons dominate the 10 GeV gamma-ray flux and pairs with $E \simeq 141$ GeV scattering off SL dominate ICS photons at 100 GeV.

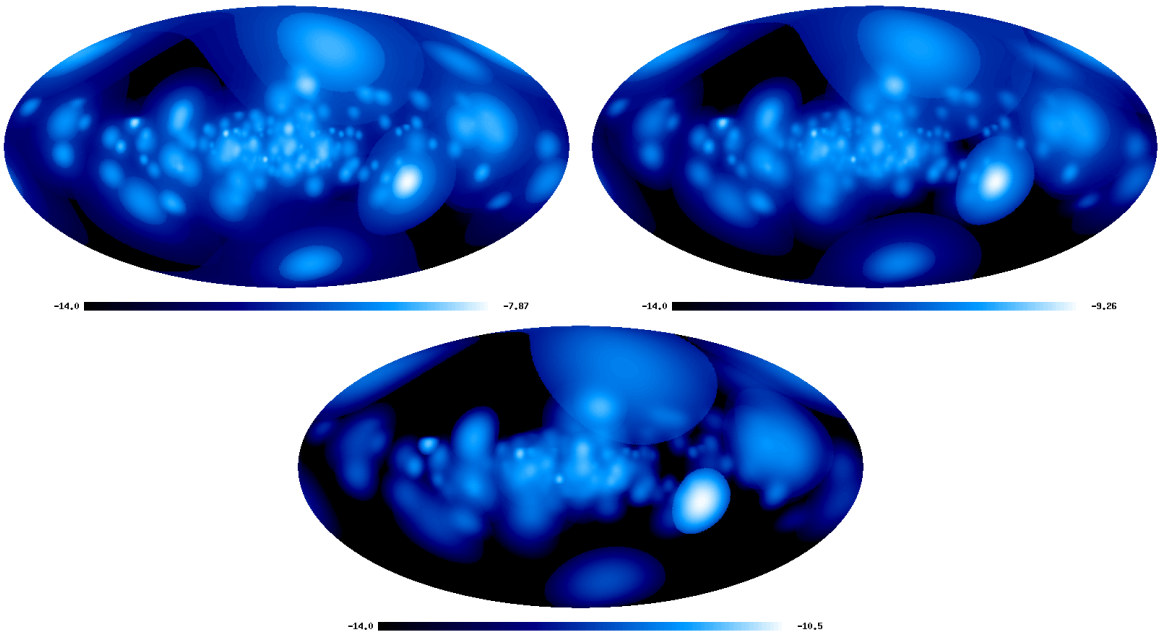

Figure 2. Sky maps of gamma-ray emission in Galactic coordinates at 1 GeV (top-left), 10 GeV (top-right) and 100 GeV (bottom) due to ICS from one realization of subhalos for the unbiased radial distribution and a minimum subhalo mass of $10^6 M_\odot$. The color scaling is logarithmic, and the unit is $1/\mathrm{s/cm^2/sr}$.

Halo model	$E_\gamma = 1$ GeV	$E_\gamma = 10$ GeV	$E_\gamma = 100$ GeV
$M_{min} = 10^{-6} M_\odot$ + unbiased	3.27×10^{-7}	2.03×10^{-8}	2.21×10^{-9}
$M_{min} = 10^{-6} M_\odot$+ anti-biased	8.17×10^{-9}	5.07×10^{-10}	5.52×10^{-11}
Host halo	3.83×10^{-10}	2.44×10^{-11}	2.73×10^{-12}

Table 1. The mean gamma-ray intensities $\langle I \rangle$ at 1 GeV, 10 GeV and 100 GeV, averaged over the sky, from subhalos with minimum mass $M_{\rm min} = 10^{-6} M_\odot$ for the unbiased and anti-biased radial distribution and from the smooth host halo. The unit is $\mathrm{cm^2/s/sr}$.

E_γ(GeV)	SL (T_p =3800 K)	IR (T_p =40.6 K)	CMB (T_p =2.73 K)
1	14 GeV (2.28 kpc)	136 GeV (1.1 kpc)	526 GeV (0.48 kpc)
10	44 GeV (1.76 kpc)	431 GeV (0.65 kpc)	1665 GeV
100	141 GeV (1.26 kpc)	1365 GeV	5267 GeV

Table 2. The dependence of the characteristic electron energy E on the energy E_γ of gamma-ray emission through inverse Compton scattering off the various black-body components of the ISRF with temperatures T_p. For the cases $E < 1$ TeV the corresponding diffusion length $\lambda_D(E)$ is also shown in braces.

In Fig. 2, we present the sky map of gamma-ray emission predicted by an unbiased radial distribution of subhalos: in order to avoid saturation from the dominant

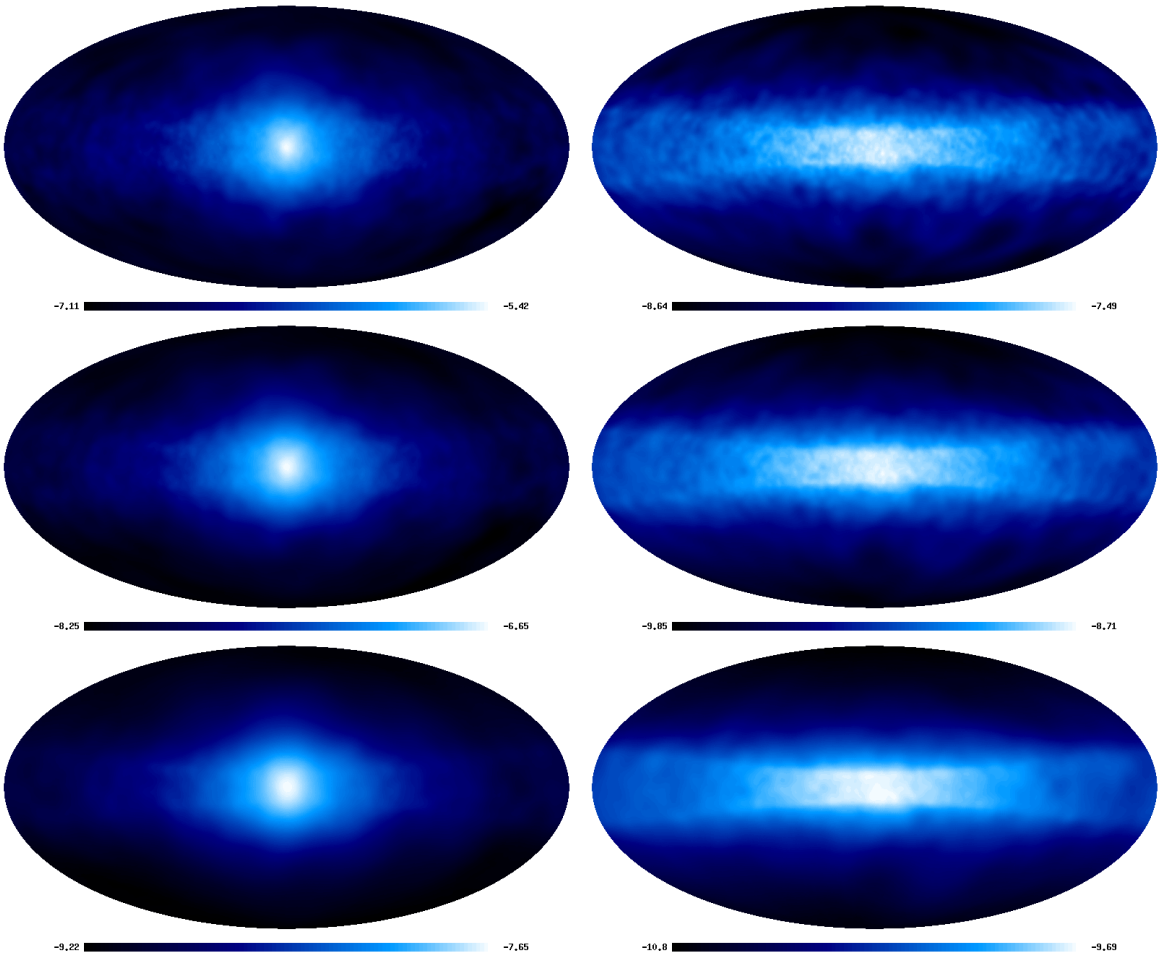

Figure 3. Sky maps of gamma-ray emission at 1 GeV, 10 GeV and 100 GeV (from top to bottom) due to ICS from one realization of subhalos for the unbiased (left panel) and anti-biased radial (right panel) distribution. The minimum subhalo mass is $10^{-6}M_{\odot}$. The color scaling is logarithmic, and the unit is $1/\mathrm{s/cm^2/sr}$.

population of small halos, in the figure we only include halos with mass above $10^6 M_{\odot}$. The most remarkable feature in Fig. 2 is that the diffuse emission regions can extend to a few kpc in length scale, corresponding to a few tens of degrees on the sky. Furthermore, the size of the brightest regions representing the largest intensity tends to increase with increasing E_γ, which could give rise to an increase of the angular power spectrum on corresponding angular scales. The size of the emitting region is basically determined by the diffusion length λ_D which is the distance that the e^+e^- diffuses during their energy loss time. This length scale can be estimated from Eq. (4), giving $\lambda_D(E) \propto E^{-0.15}$ for the MED propagation model. This energy dependence of λ_D is shown in Tab. 2. The typical diffusion length is 0.48 kpc, 0.65 kpc and 1.26 kpc for electron energies leading to emission at $E_\gamma = 1$ GeV, 10 GeV and 100 GeV, respectively, corresponding to an angular scale $\theta \simeq \lambda_D/d$ with $d \sim$ few kpc the typical distance to the dark matter annihilation source. These angular scales are roughly what one sees in Fig. 2 and the above estimate

also applies to the smooth host halo case (see Fig. 1) and to the anti-biased radial distribution of subhalos.

How does the mean intensity depend on $M_{\rm min}$? Empirically, we find that the mean intensity roughly doubles with each decade of decreasing mass of subhalos, similar to what has been found by Ref. [55]. In light of the subhalo mass function $N(>M)$ in Eq. (24) and the concentration parameter $c(M)$ in Eq. (26), the annihilation rates per decade of subhalo mass can be approximated by $L_{sub}(M)dN/d\log(M) \propto c(M)^3 MN(>M) \simeq M^{-0.3}$, which is fairly consistent with our detailed numerical calculation.

In order to determine the influence of the radial distribution of subhalos on the intensity, in Fig. 3 the gamma-ray full-sky maps at 1 GeV, 10 GeV and 100 GeV for the un-biased distribution are compared with the anti-biased distribution. For the anti-biased radial distribution the mean intensities are roughly 50 times smaller than for the unbiased case since the mean distance of subhalos to us is much larger than in the unbiased case. One notices the important feature in Fig. 3 that the emission from the spatially anti-biased distribution is much less centrally concentrated, and apparently accumulates around the Galactic plane compared with the unbiased case. This can be understood from the fact that only electrons and positrons confined within the diffusion zone of scale height $L = 4$ kpc and radius $R = 20$ kpc for the MED model can efficiently produce gamma-rays by ICS and the subhalos within the diffusion zone are distributed much more isotropically for the anti-biased case compared to the more central distribution of the unbiased case. Furthermore, ICS outside the diffusion zone contributes less than 10% to the mean intensity [38, 81, 48].

3.2. The angular power spectrum

The dimensionless angular power spectra C_l of gamma-ray emission due to the ICS at photon energies 1 GeV, 10 GeV and 100 GeV from the main components of Galactic dark matter are presented in Fig. 4. Shown are the power spectrum for subhalos with $M_{\rm min} = 10^{-6} M_\odot$ for the unbiased radial distribution and for the smooth host halo. To clearly illustrate the effects of diffusion, the angular power spectra for spatially unbiased subhalos with $M_{\rm min} = 10^2 M_\odot$ and for the host halo are also shown in absence of diffusion. We recall that in order to obtain for a given component the contribution to the angular power spectrum C_l^I in units of intensity squared, according to Eq. (29) one has to multiply the dimensionless power spectra C_l shown in Fig. 4 by the squared total intensity $\langle I \rangle^2$ of the corresponding component from Tab. 1.

Fig. 4 demonstrates the remarkable feature that the power spectrum of the ICS component of galactic dark matter annihilation is exponentially suppressed for $l \gtrsim 10$ compared with what one would obtain without diffusion. Furthermore, the lower energy gamma-rays have more angular power at $l \gtrsim 10$ corresponding to small angular scale. This can be understood from the energy-dependence of the diffusion length: Intensity fluctuations should be damped on length scales smaller than the diffusion length λ_D, corresponding to a multipole $l \gtrsim \pi d/\lambda_D$, where d is the typical distance to the dark

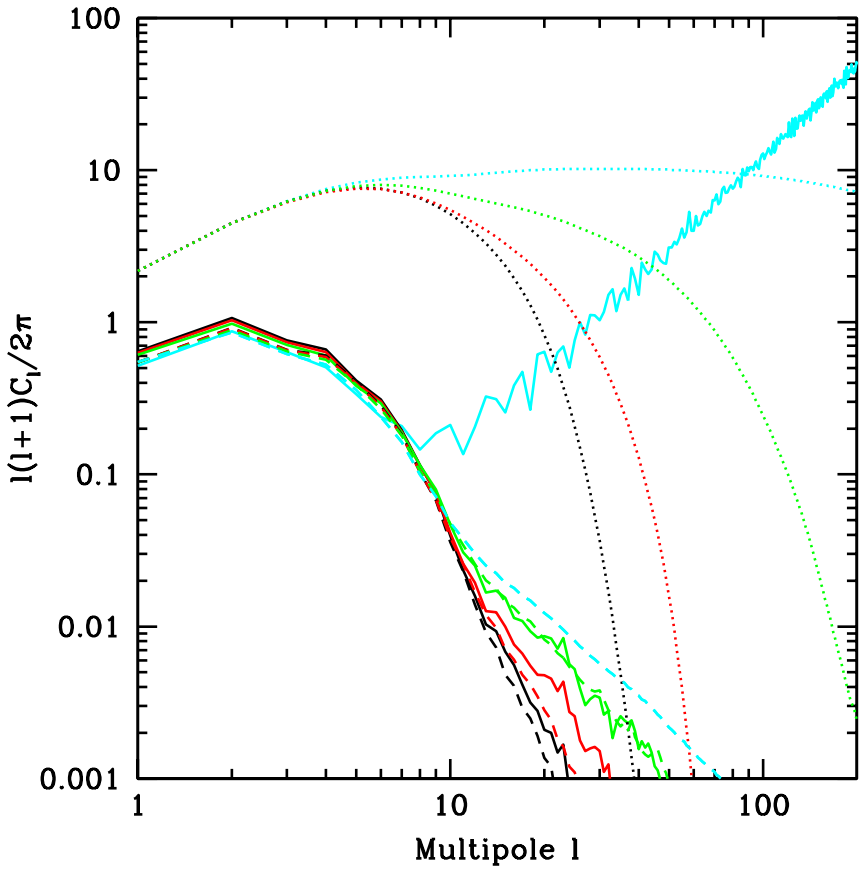

Figure 4. Dimensionless angular power spectrum C_l of the gamma-ray sky from dark matter annihilation at $E_\gamma = 1$ GeV (green), 10 GeV (red) and 100 GeV (black), respectively. Solid curves correspond to the case of substructures with minimum subhalo mass $M_{\rm min} = 10^{-6} M_\odot$ for the unbiased radial distribution. Dotted and dashed curves are for the smooth host halo with NFW profile, where the emissivity $\propto \rho^2$ and $\propto \rho$, respectively. For comparison, the cyan curves show the power spectrum in absence of diffusion, for the minimum subhalo mass $M_{\rm min} = 10^2 M_\odot$ and for the unbiased radial distribution (see text for details). We find a strong suppression due to diffusion for $l \gtrsim 10$. Each power spectrum is calculated exclusively from the contribution of the indicated source component.

matter annihilation source. Based on the discussion in Sect.3.1, we can estimate the diffusion length of the electrons and positrons emitting a given gamma-ray energy. When doing so, one should keep in mind that the e^+e^- pairs interact with three different photon backgrounds and that, as it turns out, unlike the case of a single background, the lower the gamma-ray energy the higher the energy of the emitting electrons. Since we found that the diffusion length decreases with the electron energy, $\lambda_D(E) \propto E^{-0.15}$, we expect suppression of anisotropies to occur at smaller scales, or larger values of the multipole l, for lower photon energy. For other propagation models such as the MIN and MAX models which have a slightly different energy dependence of the spatial diffusion

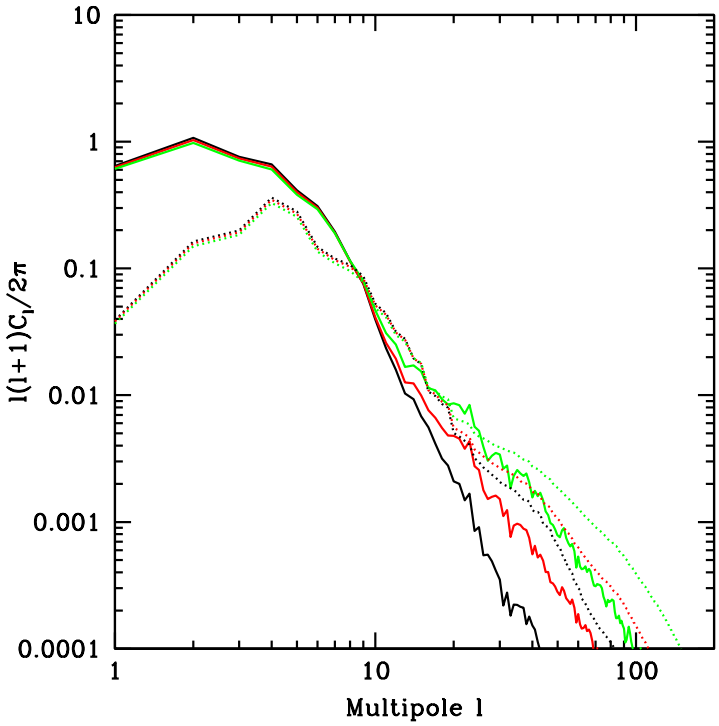

Figure 5. Comparison of the dimensionless angular power spectrum C_l of gamma-ray emission from dark matter substructures for the unbiased radial distribution (solid) and the anti-biased distribution (dotted) at $E_\gamma = 1$ GeV (green), 10 GeV (red) and 100 GeV (black) with $M_{\rm min} = 10^{-6} M_\odot$.

coefficient, the diffusion length would be slightly larger or smaller, respectively. This would shift the suppression scale in the angular power spectrum by less than a factor of two in the multipole l.

In fact, for the smooth host halo the typical distance is $d \simeq 8.5$ kpc, and the suppression due to diffusion should occur at $l \simeq 55, 47$ and 28 for gamma-ray energies of 1 GeV, 10 GeV and 100 GeV, respectively. This analysis can be applied to the case of subhalos. For an unbiased spatial distribution of subhalos, the typical distance to a subhalo is $d \simeq 7\,$kpc which corresponds to diffusive suppression at relatively smaller l compared to the host halo case. These simple estimates are consistent with our detailed calculations shown in Fig. 4.

We also find that the amplitude of the dimensionless angular power spectrum C_l from the smooth host halo is larger than that from the subhalos since the emissivity profile from annihilation in the smooth halo is proportional to the density squared and thus more peaked than annihilation in the subhalos which essentially follow the linear density profile of an NFW profile, as we see in Fig. 4. We note that although the smooth host halo has a large amplitude of the dimensionless angular power spectrum C_l, its contribution to the total intensity is as small as $\sim 0.1\%$ for the unbiased subhalo distribution and $\sim 5\%$ for the anti-biased distribution, as seen in Tab. 1. We can

therefore safely neglect the contribution from the host halo both to the mean intensity and to the dimensional angular power spectrum C_l^I.

Finally, we show in Fig. 4 the dimensionless angular power spectrum C_l for a smooth halo with emissivity tracing the density of the NFW profile instead of the squared density that would be relevant for the contribution of the host halo in decay scenarios. This shows that a smooth NFW profile describes the emission profile by a large number of subhalos following an unbiased radial distribution very well, at a level of $\sim 0.1\%$. This is not surprising since the number of subhalos within the diffusion zone with masses below $10^4 M_\odot$ is sufficiently large, $> 10^5$, for each mass decade to strongly suppress any deviation from a smooth distribution. This conclusion is also true for the anti-biased case. Despite the fact that the contribution of large subhalos in the mass range of $10^4 - 10^{10} M_\odot$ fluctuates strongly, their contribution to the total emission are three orders of magnitude smaller which leads to fluctuations at 0.1% level in angular power spectrum as seen in Fig. 4.

How does the radial subhalo distribution affect the angular power spectrum? In Fig. 5 we compare results for the unbiased case and the anti-biased case. At small l the angular power spectrum C_l for the anti-biased distribution is suppressed relative to the unbiased case which is due to the more isotropic subhalo distribution at large angular scales seen in Fig. 3. For $l \gtrsim 10$, the angular power spectrum induced by an anti-biased distribution has more power than the unbiased case because the typical distance to subhalos is larger for the anti-biased distribution, shifting power to larger l.

We should note that, of course, the electrons and positrons of ordinary astrophysical sources, such as pulsars and supernova remnants, could also produce significant ICS signals. At $l \gtrsim 10$ the corresponding angular power spectrum would be difficult to distinguish from the one induced by dark matter because the large-l power spectrum is highly suppressed and the suppression scale is mostly determined by the diffusion length of electrons and positrons which is independent of wether their origin is astrophysical or from dark matter. In contrast, the power spectrum at $l \lesssim 10$ should contain information on the sources of electrons and positrons due to the different spatial morphologies of dark matter and astrophysical sources on these scales which are not significantly influenced by diffusion. In addition, the ICS energy spectrum is in general significantly different due to the harder pair spectrum from dark matter annihilation which would naturally explain the e^+e^- excesses observed by PAMELA and Fermi-LAT. Although the nearby astrophysical sources such as pulsars can also reproduce these excesses, pulsars are mainly concentrated at the Galactic plane and the primary e^+e^- injected spectrum have an exponential cutoff at high energies, both of which are quite different from annihilating dark matter scenarios. Therefore, a combination of these two effects may allow to discriminate between astrophysical sources and at least some dark matter scenarios. For example, Ref. [82] proposed an energy dependence of an anisotropy signature to distinguish Millisecond pulsars from heavy dark matter candidates. The disentanglement of dark matter signals from astrophysical backgrounds is, however, beyond the scope of the present paper.

4. Conclusions

In this paper we have investigated the angular power spectrum of the gamma-ray emission from inverse Compton scattering off low energy target photons of electrons and positrons produced by dark matter annihilation. We considered two extreme cases for the radial distribution of subhalos and simulated the full-sky gamma-ray maps at three energies through realizations of a large number of subhalos with masses down to $10^{-6}M_{\odot}$. The contributions to the angular power spectrum and to the total flux from the smooth host halo were also calculated.

1. We point out a new feature in the angular power spectrum of photons produced by inverse Compton scattering of pairs from annihilating dark matter that does not occur in the power spectra of gamma-rays produced directly in annihilation, on which earlier work often has focused: In contrast to the direct annihilation component for which the Poisson noise dominates at large l, the angular power spectrum from inverse Compton scattering is exponentially suppressed at $l \gtrsim 10$, because the diffusion of the high energy parent electrons and positrons produced by dark matter annihilation strongly smears out anisotropies of gamma-rays at small angular scales. This suppression scale is determined by the diffusion length $\lambda_D(E)$, evaluated at the energy E of the emitting electrons and positrons. The energy E of the dominant emitters is determined by the low energy target photon backgrounds and, in the presence of several background components, is not a monotonic function of the gamma-ray energy. For the backgrounds used in this paper, CMB, IR and SL, we find that the lower energy gamma-rays are produced by the higher energy e^+e^- pairs (and vice-versa) so that when the energy dependence of the spatial diffusion coefficient is taken into account, $\lambda_D(E) \propto E^{-0.15}$, power spectrum suppression is found to occur at larger multipole l for lower photon energy.

2. The contribution to the absolute amplitude of the angular power spectrum from the smooth host halo can be safely neglected which is due to its negligible mean intensity compared to that from the subhalos. For subhalos, the intensity from an unbiased subhalo distribution is ~ 40 times larger than from an antibiased distribution. At small l the dimensionless angular power spectrum for the anti-biased distribution is suppressed relative to the unbiased case, whereas at large $l \gtrsim 10$ the opposite is true.

3. An enormous number of subhalos with the masses down to $10^{-6}M_{\odot}$ can be well described by a smooth halo whose emissivity follows the spatial distribution of subhalos. That is not surprising, because diffusion of the emitting particles can smooth the whole sky map if the number of subhalos is sufficiently large.

Finally we remark that we have assumed homogeneous and isotropic magnetic fields and interstellar radiation field. However, for the more realistic case where the radiation and magnetic fields depend on the position in the Galaxy [84], the angular power spectrum should be modified at least at large angular scales. In particular, the small scale fluctuations of the magnetic field could affect the distribution of electrons and positrons [85], influencing the angular power spectrum at all scales. Moreover, a space-dependence of the diffusion length could also lead to a directional dependence of

the angular power spectrum. Obviously detecting the differential effect of the anisotropy signal across the Galactic latitude would be even more difficult than detecting the signal integrated over the whole sky. However, it could introduce subtle effects when part of the sky is masked out, e.g. to avoid the contribution from the galactic plane. These complications should be investigated more thoroughly in the future by performing a real 3D simulation through numerically solving the transport equation for electrons and positrons. While the formalism developed in this paper can be extended to the anisotropies of the radio sky, the small scale structure of the magnetic field is more important for synchrotron emission and should be treated in more detail. In addition, our work could also be extended to inverse Compton gamma-ray emission from extragalactic dark matter halos.

Acknowledgements

We acknowledge use of the HEALPix [80] software and analysis package for deriving the results in this paper. This work was supported by the Deutsche Forschungsgemeinschaft through the collaborative research centre SFB 676 Particles, Strings and the Early Universe: The Structure of Matter and Space-Time, and by the State of Hamburg, through the Collaborative Research program Connecting Particles with the Cosmos within the framework of the Landesexzellenzinitiative (LEXI). We thank Luca Maccione and Enrico Borriello for reading the manuscript and for very useful comments.

References

[1] G. Bertone, D. Hooper and J. Silk, "Particle dark matter: Evidence, candidates and constraints," Phys. Rept. **405**, 279 (2005) [arXiv:hep-ph/0404175].

[2] G. Jungman, M. Kamionkowski and K. Griest, "Supersymmetric dark matter," Phys. Rep. **267**, 195 (1996) [arXiv:hep-ph/9506380].

[3] D. Hooper and S. Profumo, "Dark matter and collider phenomenology of universal extra dimensions," Phys. Rep. **453**, 29 (2007) [arXiv:hep-ph/0701197].

[4] E. Komatsu *et al.* [WMAP Collaboration], "Five-Year Wilkinson Microwave Anisotropy Probe Observations:Cosmological Interpretation," arXiv:0803.0547 [astro-ph].

[5] X. L. Chen and M. Kamionkowski, "Particle decays during the cosmic dark ages," Phys. Rev. D **70**, 043502 (2004) [arXiv:astro-ph/0310473].

[6] L. Zhang, X. Chen, M. Kamionkowski, Z. g. Si and Z. Zheng, "Contraints on radiative dark-matter decay from the cosmic microwave background," Phys. Rev. D **76**, 061301 (2007) [arXiv:0704.2444 [astro-ph]].

[7] L. Zhang, X. L. Chen, Y. A. Lei and Z. G. Si, "The impacts of dark matter particle annihilation on recombination and the anisotropies of the cosmic microwave background," Phys. Rev. D **74**, 103519 (2006) [arXiv:astro-ph/0603425];

[8] S. Colafrancesco, S. Profumo and P. Ullio, "Multi-frequency analysis of neutralino dark matter annihilations in the Coma cluster," Astron. Astrophys. **455**, 21 (2006) [arXiv:astro-ph/0507575].

[9] S. Profumo and P. Ullio, "Multi-wavelength Searches for Particle Dark Matter," arXiv:1001.4086 [astro-ph.HE].

[10] O. Adriani *et al.* [PAMELA Collaboration], "Observation of an anomalous positron abundance in the cosmic radiation," arXiv:0810.4995 [astro-ph].

[11] A. A. Abdo *et al.* [The Fermi-LAT Collaboration], "Measurement of the Cosmic Ray e+ plus e- spectrum from 20 GeV to 1 TeV with the Fermi Large Area Telescope," Phys. Rev. Lett. **102**, 181101 (2009) [arXiv:0905.0025 [astro-ph.HE]].

[12] F. Aharonian *et al.* [H.E.S.S. Collaboration], "The energy spectrum of cosmic-ray electrons at TeV energies," Phys. Rev. Lett. **101**, 261104 (2008) [arXiv:0811.3894 [astro-ph]].

[13] D. Grasso *et al.* [FERMI-LAT Collaboration], "On possible interpretations of the high energy electron-positron spectrum Astropart. Phys. **32** (2009) 140 [arXiv:0905.0636 [astro-ph.HE]].

[14] G. Di Bernardo, D. Gaggero, D. Grasso and f. L. collaboration, "The High Energy Cosmic Ray Electron Spectrum measured by Fermi Gamma-Ray Space Telescope: some possible interpretations," arXiv:0912.3887 [astro-ph.HE].

[15] M. Cirelli, M. Kadastik, M. Raidal and A. Strumia, "Model-independent implications of the e+, e-, anti-proton cosmic ray spectra on properties of Dark Matter," Nucl. Phys. B **813**, 1 (2009) [arXiv:0809.2409 [hep-ph]].

[16] I. Cholis, L. Goodenough, D. Hooper, M. Simet and N. Weiner, "High Energy Positrons From Annihilating Dark Matter," arXiv:0809.1683 [hep-ph].

[17] V. Barger, W. Y. Keung, D. Marfatia and G. Shaughnessy, "PAMELA and dark matter," arXiv:0809.0162 [hep-ph].

[18] R. Harnik and G. D. Kribs, "An Effective Theory of Dirac Dark Matter," arXiv:0810.5557 [hep-ph].

[19] A. E. Nelson and C. Spitzer, "Slightly Non-Minimal Dark Matter in PAMELA and ATIC," arXiv:0810.5167 [hep-ph].

[20] Y. Bai, M. Carena and J. Lykken, "The PAMELA excess from neutralino annihilation in the NMSSM," Phys. Rev. D **80**, 055004 (2009) [arXiv:0905.2964 [hep-ph]].

[21] D. Malyshev, I. Cholis and J. Gelfand, "Pulsars versus Dark Matter Interpretation of ATIC/PAMELA," arXiv:0903.1310 [astro-ph.HE].

[22] S. Profumo, "Dissecting Pamela (and ATIC) with Occam's Razor: existing, well-known Pulsars naturally account for the 'anomalous' Cosmic-Ray Electron and Positron Data," arXiv:0812.4457 [astro-ph].

[23] T. Kobayashi, Y. Komori, K. Yoshida and J. Nishimura, "The most likely sources of high energy cosmic-ray electrons in supernova remnants," Astrophys. J. **601**, 340 (2004) [arXiv:astro-ph/0308470].

[24] N. J. Shaviv, E. Nakar and T. Piran, "Natural explanation for the anomalous positron to electron ratio with supernova remnants as the sole cosmic ray source," Phys. Rev. Lett. **103**, 111302 (2009) [arXiv:0902.0376 [astro-ph.HE]].

[25] P. Blasi, "The origin of the positron excess in cosmic rays," Phys. Rev. Lett. **103**, 051104 (2009) [arXiv:0903.2794 [astro-ph.HE]].

[26] L. Bergstrom, T. Bringmann, M. Eriksson and M. Gustafsson, "Gamma rays from Kaluza-Klein dark matter," Phys. Rev. Lett. **94** (2005) 131301 [arXiv:astro-ph/0410359].

[27] F. W. B. Atwood [LAT Collaboration], "The Large Area Telescope on the Fermi Gamma-ray Space Telescope Mission," Astrophys. J. **697**, 1071 (2009) [arXiv:0902.1089 [astro-ph.IM]].

[28] J. Chiang, & R. Mukherjee, "The Luminosity Function of the EGRET Gamma-Ray Blazars," Astrophys. J. **496** (1998) 752

[29] F. W. Stecker, & M. H. Salamon, "The Gamma-Ray Background from Blazars: A New Look," Astrophys. J. **464** (1996) 600

[30] F. Miniati, "Intergalactic shock acceleration and the cosmic gamma-ray background," Mon. Not. Roy. Astron. Soc. **337** (2002) 199

[31] E. A. Baltz *et al.*, "Pre-launch estimates for GLAST sensitivity to Dark Matter annihilation signals," JCAP **0807**, 013 (2008) [arXiv:0806.2911 [astro-ph]].

[32] M. Cirelli and P. Panci, "Inverse Compton constraints on the Dark Matter e+e- excesses," Nucl. Phys. B **821**, 399 (2009) [arXiv:0904.3830 [astro-ph.CO]].

[33] E. A. Baltz and L. Wai, "Diffuse inverse Compton and synchrotron emission from dark matter annihilations in galactic satellites," Phys. Rev. D **70**, 023512 (2004) [arXiv:astro-ph/0403528].

[34] Q. Yuan, P. F. Yin, X. J. Bi, X. M. Zhang and S. H. Zhu, "Gamma rays and neutrinos from dark matter annihilation in galaxy clusters," Phys. Rev. D **82**, 023506 (2010) [arXiv:1002.0197 [astro-ph.HE]].

[35] C. Boehm, T. Delahaye and J. Silk, "Can the morphology of gamma-ray emission distinguish annihilating from decaying dark matter?," arXiv:1003.1225 [astro-ph.GA].

[36] G. Hutsi, A. Hektor and M. Raidal, "Implications of the Fermi-LAT diffuse gamma-ray measurements on annihilating or decaying Dark Matter," JCAP **1007**, 008 (2010) [arXiv:1004.2036 [astro-ph.HE]].

[37] T. Lin, D. P. Finkbeiner and G. Dobler, "The Electron Injection Spectrum Determined by Anomalous Cosmic Ray, Gamma Ray, and Microwave Signals," arXiv:1004.0989 [astro-ph.CO].

[38] L. Zhang, G. Sigl and J. Redondo, "Galactic Signatures of Decaying Dark Matter," JCAP **0909**, 012 (2009) [arXiv:0905.4952 [astro-ph.GA]].

[39] L. Zhang, C. Weniger, L. Maccione, J. Redondo and G. Sigl, "Constraining Decaying Dark Matter with Fermi LAT Gamma-rays," JCAP **1006**, 027 (2010) [arXiv:0912.4504 [astro-ph.HE]].

[40] A. M. Green, S. Hofmann and D. J. Schwarz, "The first WIMPy halos," JCAP **0508**, 003 (2005) [arXiv:astro-ph/0503387].

[41] A. Loeb and M. Zaldarriaga, "The small-scale power spectrum of cold dark matter," Phys. Rev. D **71**, 103520 (2005) [arXiv:astro-ph/0504112].

[42] E. Bertschinger, "The effects of cold dark matter decoupling and pair annihilation on cosmological perturbations," Phys. Rev. D **74**, 063509 (2006) [arXiv:astro-ph/0607319].

[43] S. Profumo, K. Sigurdson and M. Kamionkowski, "What mass are the smallest protohalos?," Phys. Rev. Lett. **97**, 031301 (2006) [arXiv:astro-ph/0603373].

[44] J. Diemand, B. Moore and J. Stadel, "Earth-mass dark-matter haloes as the first structures in the early universe," Nature **433**, 389 (2005) [arXiv:astro-ph/0501589].

[45] L. Gao *et al.*, "The redshift dependence of the structure of massive LCDM halos," arXiv:0711.0746 [astro-ph].

[46] L. Gao, S. D. M. White, A. Jenkins, F. Stoehr and V. Springel, "The subhalo populations of LCDM dark haloes," Mon. Not. Roy. Astron. Soc. **355**, 819 (2004) [arXiv:astro-ph/0404589].

[47] J. Diemand, M. Kuhlen and P. Madau, "Dark matter substructure and gamma-ray annihilation in the Milky Way halo," Astrophys. J. **657**, 262 (2007) [arXiv:astro-ph/0611370].

[48] J. M. Cline, A. C. Vincent and W. Xue, "Leptons from Dark Matter Annihilation in Milky Way Subhalos," Phys. Rev. D **81**, 083512 (2010) [arXiv:1001.5399 [astro-ph.CO]].

[49] L. Pieri, G. Bertone and E. Branchini, "Dark Matter Annihilation in Substructures Revised," Mon. Not. Roy. Astron. Soc. **384**, 1627 (2008) [arXiv:0706.2101 [astro-ph]].

[50] M. Kamionkowski, S. M. Koushiappas and M. Kuhlen, "Galactic Substructure and Dark Matter Annihilation in the Milky Way Halo," Phys. Rev. D **81**, 043532 (2010) [arXiv:1001.3144 [astro-ph.GA]].

[51] S. Ando and E. Komatsu, "Anisotropy of the cosmic gamma-ray background from dark matter annihilation," Phys. Rev. D **73** (2006) 023521 [arXiv:astro-ph/0512217].

[52] S. Ando, E. Komatsu, T. Narumoto and T. Totani, "Dark matter annihilation or unresolved astrophysical sources? Anisotropy probe of the origin of cosmic gamma-ray background," Phys. Rev. D **75**, 063519 (2007) [arXiv:astro-ph/0612467].

[53] S. Ando, "Gamma-ray background anisotropy from galactic dark matter substructure," arXiv:0903.4685 [astro-ph.CO].

[54] L. Zhang and G. Sigl, "Dark Matter Signatures in the Anisotropic Radio Sky," JCAP **0809**, 027 (2008) [arXiv:0807.3429 [astro-ph]].

[55] J. M. Siegal-Gaskins, "Revealing dark matter substructure with anisotropies in the diffuse gamma-ray background," JCAP **0810**, 040 (2008) [arXiv:0807.1328 [astro-ph]].

[56] M. Fornasa, L. Pieri, G. Bertone and E. Branchini, "Anisotropy probe of galactic and extra-galactic Dark Matter annihilations," arXiv:0901.2921 [astro-ph].

[57] A. Cuoco, J. Brandbyge, S. Hannestad, T. Haugboelle and G. Miele, "Angular Signatures of

Annihilating Dark Matter in the Cosmic Gamma-Ray Background," Phys. Rev. D **77** (2008) 123518 [arXiv:0710.4136 [astro-ph]].

[58] J. M. Siegal-Gaskins and V. Pavlidou, "Robust identification of isotropic diffuse gamma rays from Galactic dark matter," arXiv:0901.3776 [astro-ph.HE].

[59] B. S. Hensley, J. M. Siegal-Gaskins and V. Pavlidou, "The detectability of dark matter annihilation with Fermi using the anisotropy energy spectrum of the gamma-ray background," arXiv:0912.1854 [astro-ph.CO].

[60] J. Zavala, V. Springel and M. Boylan-Kolchin, "Extragalactic gamma-ray background radiation from dark matter annihilation," Mon. Not. Roy. Astron. Soc. **405**, 593 (2010) [arXiv:0908.2428 [astro-ph.CO]].

[61] F. Miniati, "Numerical modelling of gamma radiation from galaxy clusters," Mon. Not. Roy. Astron. Soc. **342**, 1009 (2003)

[62] F. Miniati, S. M. Koushiappas and T. Di Matteo, "Angular Anisotropies in the Cosmic Gamma-ray Background as a Probe of its Origin," Astrophys. J. **667** (2007) L1 [arXiv:astro-ph/0702083].

[63] V. Pavlidou and B. D. Brian, "The Guaranteed Gamma-Ray Background," Astrophys. J. **575** (2002) L5

[64] S. Ando and V. Pavlidou, "Imprint of galaxy clustering in the cosmic gamma-ray background," Mon. Not. Roy. Astron. Soc. **400** (2009) 2122 [arXiv:0908.3890 [astro-ph.HE]].

[65] A. Cuoco, A. Sellerholm, J. Conrad and S. Hannestad, "Anisotropies in the Diffuse Gamma-Ray Background from Dark Matter with Fermi LAT: a closer look," arXiv:1005.0843 [astro-ph.HE].

[66] R. Schlickeiser, *Cosmic Ray Astrophysics* (2002) (Berlin: Springer)

[67] T. Delahaye, F. Donato, N. Fornengo, J. Lavalle, R. Lineros, P. Salati and R. Taillet, "Galactic secondary positron flux at the Earth," Astron. Astrophys. **501**, 821 (2009) [arXiv:0809.5268 [astro-ph]].

[68] F. Donato, D. Maurin, P. Salati, A. Barrau, G. Boudoul and R. Taillet, "Antiprotons from spallation of cosmic rays on interstellar matter," Astrophys. J. **563**, 172 (2001) [arXiv:astro-ph/0103150].

[69] T. Delahaye, J. Lavalle, R. Lineros, F. Donato and N. Fornengo, "Galactic electrons and positrons at the Earth:new estimate of the primary and secondary fluxes," arXiv:1002.1910 [astro-ph.HE].

[70] Strong A.W. and Moskalenko I.W., "Propagation of cosmic-ray nucleons in the Galaxy," Astrophys. J. **509** (1998) 212 [astro-ph/9807150].

[71] T. A. Porter, I. V. Moskalenko and A. W. Strong, "Inverse Compton emission from galactic supernova remnants: Effect of the interstellar radiation field," Astrophys. J. **648**, L29 (2006) [arXiv:astro-ph/0607344].

[72] T. Delahaye, R. Lineros, F. Donato, N. Fornengo and P. Salati, "Positrons from dark matter annihilation in the galactic halo: theoretical uncertainties," Phys. Rev. D **77**, 063527 (2008) [arXiv:0712.2312 [astro-ph]].

[73] D. Maurin, F. Donato, R. Taillet and P. Salati, "Cosmic Rays below Z=30 in a diffusion model: new constraints on propagation parameters," Astrophys. J. **555**, 585 (2001) [arXiv:astro-ph/0101231].

[74] Rybicki G.B., Lightman A.P., Radiative Processes in Astrophysics, 1979, John Wiley & Sons.

[75] O. Petruk, "Approximation for radiation power of electrons due to inverse-Compton process in the black-body photon field," arXiv:0807.1969 [astro-ph].

[76] J. F. Navarro, C. S. Frenk and S. D. M. White, "The Structure of Cold Dark Matter Halos," Astrophys. J. **462**, 563 (1996) [arXiv:astro-ph/9508025].

[77] N. Fornengo, L. Pieri and S. Scopel, "Neutralino annihilation into gamma-rays in the Milky Way and in external galaxies," Phys. Rev. D **70**, 103529 (2004) [arXiv:hep-ph/0407342].

[78] J. Diemand, M. Kuhlen and P. Madau, "Formation and evolution of galaxy dark matter halos and their substructure," Astrophys. J. **667**, 859 (2007) [arXiv:astro-ph/0703337].

[79] J. S. Bullock *et al.*, "Profiles of dark haloes: evolution, scatter, and environment," Mon. Not. Roy. Astron. Soc. **321**, 559 (2001) [arXiv:astro-ph/9908159].

[80] K. M. Gorski, E. Hivon, A. J. Banday, B. D. Wandelt, F. K. Hansen, M. Reinecke and M. Bartelman, "HEALPix – a Framework for High Resolution Discretization, and Fast Analysis of Data Distributed on the Sphere," Astrophys. J. **622**, 759 (2005) [arXiv:astro-ph/0409513].

[81] M. Perelstein and B. Shakya, "Comment on Calculation of Positron Flux from Galactic Dark Matter," arXiv:1002.4588 [astro-ph.HE].

[82] J. M. Siegal-Gaskins, R. Reesman, V. Pavlidou, S. Profumo and T. P. Walker, "Anisotropy Constraints on Millisecond Pulsars in the Diffuse Gamma Ray Background," arXiv:1011.5501 [astro-ph.HE].

[83] G. Dobler, D. P. Finkbeiner, I. Cholis, T. R. Slatyer and N. Weiner, "The Fermi Haze: A Gamma-Ray Counterpart to the Microwave Haze," Astrophys. J. **717**, 825 (2010) [arXiv:0910.4583 [astro-ph.HE]].

[84] Heiles, Carl, "The Local Direction and Curvature of the Galactic Magnetic Field Derived from Starlight Polarization," Astrophys. J. **462**, 316 (1996).

[85] X. L. Chen, "Angular power spectrum of the galactic synchrotron radiation," arXiv:astro-ph/0409733.